Title

Numerical Evaluation of Flow and Heat Transfer in Plate-Pin Fin Heat Sinks with Various Pin Cross-Sections

Journal

Numerical Heat Transfer, Part A: Applications, 60(2)

ISSN

1040-7782 1521-0634

Authors

Zhou, Feng
Catton, Ivan

Publication Date

2011-07-15

DOI

10.1080/10407782.2011.588574

Peer reviewed

Numerical Heat Transfer, Part A: Applications

Publication details, including instructions for authors and subscription information:
http://www.tandfonline.com/loi/unht20

Numerical Evaluation of Flow and Heat Transfer in Plate-Pin Fin Heat Sinks with Various Pin Cross-Sections

Feng Zhou [a b] & Ivan Catton [b]

[a] School of Energy and Environment, Southeast University, Nanjing, P.R. China

[b] Department of Mechanical and Aerospace Engineering, University of California, Los Angeles, California, USA

Available online: 05 Jul 2011

To cite this article: Feng Zhou & Ivan Catton (2011): Numerical Evaluation of Flow and Heat Transfer in Plate-Pin Fin Heat Sinks with Various Pin Cross-Sections, Numerical Heat Transfer, Part A: Applications, 60:2, 107-128

To link to this article: http://dx.doi.org/10.1080/10407782.2011.588574

Numerical Heat Transfer, Part A, 60: 107–128, 2011

ISSN: 1040-7782 print/1521-0634 online
DOI: 10.1080/10407782.2011.588574

Taylor & Francis
Taylor & Francis Group

NUMERICAL EVALUATION OF FLOW AND HEAT TRANSFER IN PLATE-PIN FIN HEAT SINKS WITH VARIOUS PIN CROSS-SECTIONS

Feng Zhou[1,2] and Ivan Catton[2]

[1]*School of Energy and Environment, Southeast University, Nanjing, P.R. China*

[2]*Department of Mechanical and Aerospace Engineering, University of California, Los Angeles, California, USA*

A numerical investigation of the thermal and hydraulic performance of 20 different plate-pin fin heat sinks with various shapes of pin cross-sections (square, circular, elliptic, NACA profile, and dropform) and different ratios of pin widths to plate fin spacing (0.3, 0.4, 0.5, and 0.6) was performed. Finite volume method-based CFD software, Ansys CFX, was used as the 3-D Reynolds-averaged Navier-Stokes Solver. A k-ω based shear-stress-transport model was used to predict the turbulent flow and heat transfer through the heat sink channels. The present study provides original information about the performance of this new type of compound heat sink.

1. INTRODUCTION

The challenge posed by high heat fluxes in electronic chips makes thermal management an essential element in the development of these systems, which are driving conflicting needs for high performance as well as reduced power consumption, size, and weight. Although many new cooling technologies such as cooling by heat pipes, cold water, and even by liquid nitrogen have been proposed and adopted, air cooling by heat sink is still a commonly used solution for thermal management in electronic packaging due to its low cost, availability, and reliability factors. In the electronic thermal management, heat sinks are usually attached on the tops of the electronic packages to enhance heat dissipation and control junction temperatures of these packages. The overall objective of the heat sink design is significant enhancement of convective heat transfer with minimal increases in the streamwise pressure drop penalties.

Received 3 September 2010; accepted 16 April 2011.

The support of a DARPA grant within the MACE program is gratefully acknowledged. The views, opinions, and/or findings contained in this article are those of the author and should not be interpreted as representing the official views or policies, either expressed or implied, of the Defense Advanced Research Projects Agency or the Department of Defense.

Address correspondence to Feng Zhou, Department of Mechanical Engineering, University of California, Los Angeles, 48-121 Engineering IV, 420 Westwood Plaza, Los Angeles, CA, 900095-1597, USA. E-mail: zhoufeng@ucla.edu

NOMENCLATURE

a	length of long axis or chord length, m	S_f	spacing between the plate fins, m
A_p	power applied area, m^2	T	temperature, K
b	length of short axis, m	ΔT	temperature difference, K
CB	width of wind tunnel duct with no bypass, m	u	vector of velocity, m/s
		uc	wind velocity through the channel, m/s
CH	height of wind tunnel duct with no bypass, m	u_{in}	velocity at the inlet, m/s
		y	the distance to the nearest wall, m
d	pin diameter of the pin fin heat sink, m	**Greek**	
D	pin diameter of the plate-pin fin heat sink, m	α, β, β^*	turbulence model constant
		δ_f	thickness of a fin, m
D_h	hydraulic diameter, m	η_{eff}	heat transfer effectiveness factor
f	friction factor	λ_f	thermal conductivity of the fluid, $W/(m \cdot K)$
F_1, F_2	blending function		
H	height of the heat sinks, m	μ	viscosity, $Pa \cdot s$
H_b	height of the base, m	μ_t	turbulent eddy viscosity, $Pa \cdot s$
H_f	height of the fin, m	ν	kinematic viscosity, m^2/s
k	turbulence kinetic energy per unit mass, m^2/s^2	ν_t	turbulent kinematic viscosity, m^2/s
		ρ	density, kg/m^3
L	length of the fin, m	σ_ϵ	k-ϵ turbulence model constant
Nu	nusselt number	σ_k	turbulence model constant for the k equation
Δp	pressure drop, Pa		
P_k	shear production of turbulence	σ_ω	k-ω turbulence model constant
P_l	pin pitch in streamwise direction, m	ϕ	represent any constant in the original k-ω model (σk_1, ...)
P_r	prandtl number		
P_{rt}	turbulent Prandtl number	ϕ	represent any constant in the transformed k-ε model (σk_2, ...)
Q	power applied on the base, W		
R_1, R_2	radii of the dropform shape, m	ϕ	represent the corresponding constant in the SST model (σk, ...)
Re	reynolds number		
R_{th}	thermal resistance, K/W	ω	specific turbulence dissipation rate
S	an invariant measure of the strain rate		

Among the varieties of heat sinks, plate fin heat sinks (PFHSs) are the most widely used due to their simple structure and easy manufacturing. Many publications have investigated the modeling and optimization of the PFHS to determine the optimum fin height, fin pitch, and fin thickness to obtain maximum heat dissipation. Knight et al. [1, 2] presented a scheme to determine the dimensions of a microchannel heat sink that will minimize the thermal resistance using conservation equations presented in a generalized, dimensionless form along with applicable geometrical relationships. They [3] then used the optimization scheme to design, build and test several air cooled aluminium finned arrays. Teertstra et al. [4]. presented an analytical model to predict the average heat transfer rate for forced convection, air cooled, plate fin heat sinks for electronics applications. Copeland [5] calculated the optimum dimensions of fin thickness and pitch for a variety of realistic operating conditions, using an analytical model. Culham and Muzychka [6] presented a procedure that allows the simultaneous optimization of heat sink design parameters based on a minimization of the entropy generation associated with heat transfer and fluid friction. Iyengar and Bar-Cohen [7] provided a viable technique for combining least-material optimization with the entropy minimization methodology by a coefficient of performance (COP_T) analysis for plate fin heat sinks in forced

convection. Chiang [8] presented an effective method for predicting and optimizing the cooling performance of a plate fin heat sink module based on the Taguchi method. All of the above investigations are focused on the optimization of plate fin heat sinks and show that the performance of PFHSs can be increased to a certain extent by adopting optimum geometries. However, the optimization procedures cannot overcome the intrinsic shortcoming in the structure of a PFHS, i.e., air flows smoothly through the heat sink channels due to the parallel plate fin arrangement, which leaves room for further study on enhancing the heat transfer performance of PFHSs.

Pin fin heat sinks are another efficient heat transfer device used in many electronic cooling applications. There are many publications on heat transfer in electronic cooling using pin fin heat sinks. Sparrow et al. [9] performed heat transfer and pressure drop experiments for in-line pin fin arrays to obtain basic data to complement available information for staggered arrays. Sparrow and Kang [10] performed heat transfer and pressure drop experiments for cross-flow tube banks in which the individual tubes were equipped with longitudinal fins. Sparrow and Grannis [11] performed a broad-ranging investigation encompassing complementary experimentation and numerical simulation to determine the pressure drop characteristics of diamond-shaped pin fins. Chapman et al. [12] designed elliptical pin fin heat sinks to minimize the pressure loss and enhance the thermal performance. Li et al [13]. carried out experiments to investigate heat transfer and flow resistance characteristics in rectangular ducts with staggered arrays of short elliptic pin fins in a cross-flow of air. Yang et al. [14] performed an experimental study of pin fin heat sinks having circular, elliptic, and square cross-sections. Horvat and Catton [15, 16] developed a fast running computational algorithm based on the volume averaging theory (VAT) to simulate conjugate heat transfer process in a pin fin heat sink, which offers possibilities for geometry improvements and optimization to achieve higher thermal effectiveness. Park et al. [17] performed the design optimization of a 7×7 pin fin heat sink numerically to achieve higher thermal performance of the heat sink using the weighting method for predicting the multiobjective problem. Chen et al. [18] developed an effective method for performing the thermal optimization of fully confined pin fin heat sinks under constraints of pressure drop, mass, and space limitations. Khan et al. [19, 20] studied the thermodynamic losses caused by heat transfer and pressure drop in cylindrical pin fin heat sinks by applying an entropy generation minimization (EGM) technique, which allows all relevant design parameters for pin-fin heat sinks, including geometric parameters, material properties and flow conditions, to be simultaneously optimized. Chiang et al. [21, 22] explored the optimal values of designing parameters of a pin fin type heat sink under constrains of mass and space limitation to achieve high thermal performance (or cooling efficiency) by experiment. There are also some publications on comparisons of fluid flow and thermal characteristics of plate fin and pin fin heat sinks. Jonsson and Moshfegh [23] conducted tests in a wind tunnel with seven types of heat sinks including plate fin, strip fin, and pin fin heat sinks. An empirical bypass correlation has been developed for the different fin designs. Soodphakdee et al. [24] compared the heat transfer performance of various commonly used fin geometries, which include plate fins (parallel plates and staggered plates) and pin fins (round, elliptical and square). It was concluded that the staggered plate fin geometry showed the highest heat transfer for a given combination of pressure gradient and flow rate. Kin et al.

[25] compared the thermal performances of plate fin and pin fin heat sinks and proposed correlations for the friction factor and Nusselt number for each type of heat sink. Compared with plate fin heat sinks which have the advantages of simple structure and easy manufacturing, pin fin heat sinks have an advantage of hindering the development of a thermal boundary layer at the expense of an increased pressure drop.

To overcome the intrinsic shortcomings in structures of PFHSs mentioned above, which is undesirable for enhancing heat transfer performances of heat sinks, Yu et al. [26–28] developed a new compound heat sink based on the plate fin heat sink, by placing circular pin fins into the flow channels to increase the turbulence. Yang and Peng [29] used numerical solutions to compare the thermal and hydraulic performances of both circular and square Plate-pin fin heat sinks (PPFHS) with plate fin heat sink. It was found that the thermal resistance of compound heat sinks was lower than PFHS at the same flow velocity. However, the pressure drop of the compound heat sink is much higher than the PFHS. To overcome the shortcomings in structure of plate-pin fin heat sinks, mixed-height pins were used by Yang and Peng [30] in a subsequent work to improve the hydraulic performance. The synthetical performance of the PPFHS with mixed-height pins was better than the original circular plate-pin fin heat sink, but the improvement was quite limited.

The present article describes an effort to improve the synthetical performance of this new type of compound heat sink by employing pin fins with various shapes of cross-sections (square, circular, elliptic, NACA 0050 profile, and dropform), and different ratios of pin widths to plate fin spacing (0.3, 0.4, 0.5, and 0.6). The thermal and hydraulic performance of these PPFHSs was compared with plate fin and pin fin heat sinks in terms of Nusselt number, pressure drop, and heat transfer effectiveness factor. In the following presentation, the experimental results by Jonsson and Moshfegh [23] for plate fin and pin fin heat sinks and by Yu [28] for a circular PPFHS are first numerically simulated to verify and validate the numerical model and CFD code. After that, 20 PPFHS models with different forms of pin cross-sections and pin widths, including the plate fin and pin fin heat sinks, are numerically simulated and compared from three different aspects at various wind velocities. The first is a qualitative comparison to give insight into the flow behavior and temperature distribution around the pins. The second is a quantitative comparison of heat transfer enhancements and pressure drop penalties. The third is a comprehensive comparison from the viewpoint of overall performance or heat dissipation efficiency. Finally, some conclusions are drawn that should be helpful in the design of heat sinks.

2. NUMERICAL METHOD AND PROCEDURES

2.1. Physical Model

Schematic diagrams of the plate fin and pin fin heat sinks having the same fin spacing and fin thickness were experimentally compared by Jonsson and Moshfegh [23], shown in Figures 1*a* and 1*b*. These two commonly used heat sinks are adopted to calculate a baseline for the flow characteristics and heat transfer performance. The circular plate-pin fin heat sink tested by Yu [28] is shown in Figure 1*c*. All of the heat sinks are fully-shrouded and the top surface is insulated. The dimensions of the heat sinks are tabulated in Table 1.

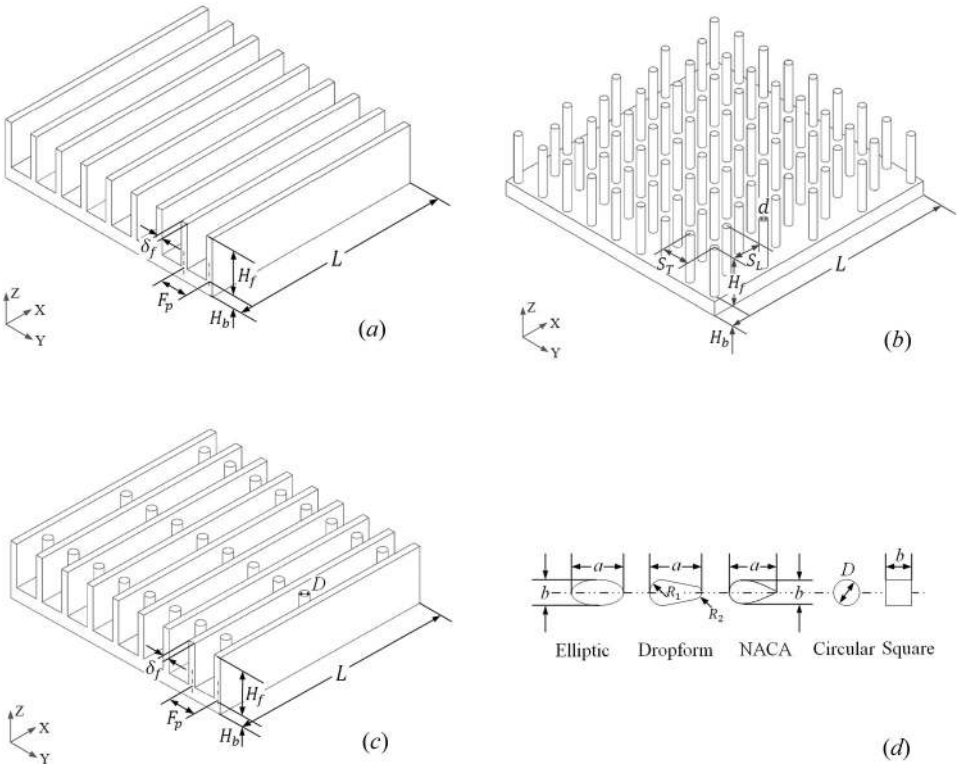

Figure 1. Some schematic diagram: (*a*) Plate fin heat sink; (*b*) pin fin heat sink; (*c*) plate-pin fin heat sink; and (*d*) cross-sections of the five types of pins.

Besides circular pins, four other types of pins having elliptic, dropform, NACA 0050 profiles [31–33], and square cross-sections are adopted to build different kinds of plate-pin fin heat sinks, as shown in Figure 1*d*. In order to provide a fair and physically meaningful basis for the comparison, the areas projected in the flow direction or the flow blockage areas are kept the same, which means the width of all the pins b, is set to be equal to the diameter of the circular pin D. The pitch between adjacent pin fins and the pin length are also kept the same.

To make the comparisons more generalized and to see how the dimensionless width of the pins b/S_f effects the performance of the PPFHSs, the widths of all five

Table 1. Dimensions of the heat sinks

	Parameters	mm		Parameters	mm
L	Length of the plate fin	51	H_f	Height of the fin	10
H_b	Height of the base	3	S_f	Plate fin spacing	5
δ_f	Plate fin thickness	1.5	F_p	Plate fin pitch	6.5
S_T	Transverse pitch of pin fins	6.5	S_L	Longitudinal pitch of pin fins	6.5
D	Pin diameter of PPFHS	1.5, 2, 2.5, 3	d	Pin diameter of pin fin HS	1.5

types of pins are 1.5 mm, 2 mm, 2.5 mm, and 3 mm, with the corresponding values of b/S_f, being 0.3, 0.4, 0.5, and 0.6. In total, 22 types of heat sink models, including the plate fin and pin fin heat sinks, are numerically tested and compared at four different velocities, ranging from 6.5 m/s to 12.2 m/s. The dimensions of the pins are tabulated in Table 2.

2.2. Mathematical Model

In this study, the flow is assumed to be three-dimensional, incompressible, steady state, and turbulent. Buoyancy and radiation heat transfer effects are not taken into consideration. The three-dimensional governing equations for continuity, momentum, and energy are as follows [34–36].

Continuity equation

$$\frac{\partial \rho u_i}{\partial x_i} = 0 \tag{1}$$

Momentum equation

$$\rho u_j \frac{\partial u_i}{\partial x_j} = \frac{\partial}{\partial x_j}\left[(\mu + \mu_t)\frac{\partial u_i}{\partial x_j}\right] - \frac{\partial p}{\partial x_i} \tag{2}$$

Energy equation

$$\rho u_j \frac{\partial T}{\partial x_j} = \frac{\partial}{\partial x_j}\left[\left(\frac{\mu}{\mathrm{Pr}} + \frac{\mu_t}{\mathrm{Pr}_t}\right)\frac{\partial T}{\partial x_j}\right] \tag{3}$$

The k–ω-based shear-stress-transport (SST) model with automatic wall function treatment [37] is used to predict the turbulent flow and heat transfer along the heat sink channel. The model blends the robust and accurate formulation of the k–ω model in the near-wall region with the free-stream independence of the k–ε model in the far field. The SST model gives a highly accurate prediction of the onset and the amount of flow separation under adverse pressure gradients by the inclusion of transport effects into the formulation of the eddy-viscosity [38]. This results in a major improvement in terms of flow separation predictions. The superior performance of the SST model has been demonstrated for high accuracy boundary layer simulations in a large number of validation studies.

Table 2. Dimensions of the pins

	Dimensions of pins			
b/S_f	a	b	R_1	R_2
0.3	3	1.5	0.75	0.225
0.4	4	2	1	0.3
0.5	5	2.5	1.25	0.375
0.6	6	3	1.5	0.45

Menter [39, 40] proposed the equations for the SST model as

$$\frac{D(\rho k)}{Dt} = \widetilde{P}_k - \beta^* \rho k\omega + \frac{\partial}{\partial x_j}\left[(\mu + \sigma_k \mu_t)\frac{\partial k}{\partial x_i}\right] \tag{4}$$

$$\frac{D(\rho\omega)}{Dt} = \alpha\rho S^2 - \beta\rho\omega^2 + \frac{\partial}{\partial x_i}\left[(\mu + \sigma_\omega \mu_t)\frac{\partial \omega}{\partial x_i}\right] + 2(1 - F_1)\rho\sigma_{\omega_2}\frac{1}{\omega}\frac{\partial k}{\partial x_i}\frac{\partial \omega}{\partial x_i} \tag{5}$$

where the blending function F_1 is defined by

$$F_1 = \tan h\left\{\left\{\min\left[\max\left(\frac{\sqrt{k}}{\beta^*\omega y}, \frac{500\nu}{y^2\omega}\right), \frac{4\rho\sigma_{\omega_2}k}{CD_{k\omega}y^2}\right]\right\}^4\right\} \tag{6}$$

in which

$$CD_{k\omega} = \max\left(2\rho\sigma_{\omega_2}\frac{1}{\omega}\frac{\partial k}{\partial x_j}\frac{\partial \omega}{\partial x_j}, 10^{-10}\right) \tag{7}$$

The turbulent eddy viscosity is computed from

$$\nu_t = \frac{a_1 k}{\max(a_1\omega, SF_2)} \tag{8}$$

where S is the invariant measure of the strain rate and F_2 is a second blending function defined by

$$F_2 = \tan h\left\{\left[\max\left(2\frac{\sqrt{k}}{\beta^*\omega y}, \frac{500\nu}{y^2\omega}\right)\right]^2\right\} \tag{9}$$

To prevent the build-up of turbulence in stagnation regions, a production limiter is used in the SST model.

$$P_k = \mu_t \frac{\partial u_i}{\partial x_j}\left(\frac{\partial u_i}{\partial x_j} + \frac{\partial u_j}{\partial x_i}\right) \rightarrow \widetilde{P}_k = \min(P_k, 10 \cdot \beta^* \rho k\omega) \tag{10}$$

Each of the constants is a blend of the corresponding constants of the k-ϵ and the k-ω model.

$$\phi = F_1\phi_1 + (1 - F_1)\phi_2 \tag{11}$$

The constants for this model take the following values.

$$\begin{aligned} &\beta^* = 0.09 \\ &\alpha_1 = 5/9, \beta_1 = 3/40, \sigma_{k1} = 0.85, \sigma_{\omega 1} = 0.5 \\ &\alpha_2 = 0.44, \beta_2 = 0.0828, \sigma_{k2} = 1, \sigma_{\omega 2} = 0.856 \end{aligned} \tag{12}$$

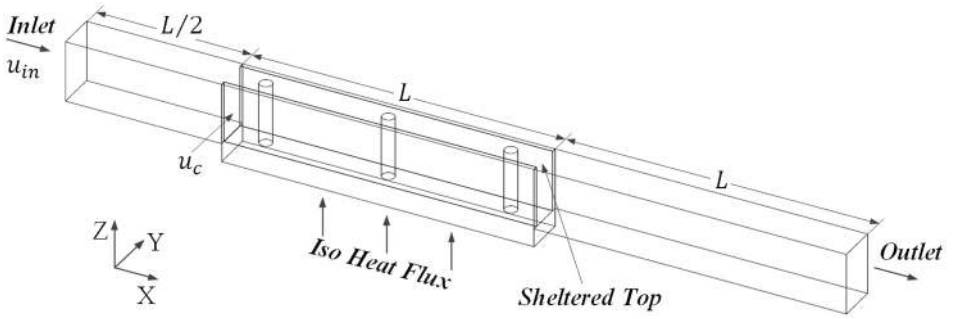

Figure 2. Computational domain.

A commercial finite volume method (FVM)-based code, CFX 12.1 [41], is used to analyze the turbulent convective heat transfer in a three-dimensional channel of the heat sinks. This code solves the Reynolds-averaged Navier–Stokes equations with a high resolution scheme for the advection terms as well as turbulence numerics. The fully coupled momentum and energy equations are solved simultaneously. The RMS type residual for solution convergence criteria is set to be 10^{-5} for the momentum balance and 10^{-6} for the energy equation.

2.3. Computational Domain and Grid System

Since the fin geometry is periodic in the spanwise direction, a single passage between the midlines of two proximate fins of the heat sink is selected to be the computational domain (see Figure 2). Because of the thickness of the fin, the air velocity profile at the entrance of the channel is not uniform. The computational domain is then extended upstream 0.5 times the streamwise fin length, and the downstream boundary of the computational domain is located at the distance of a fin length from the trailing edge of the fin in the streamwise direction.

The velocity boundary condition and a constant temperature is set at the domain inlet. The turbulence intensity of the flow entering through the inlet boundary is set to 5%. The velocity at the inlet of extended region, u_{in} changed from 5 m/s to 9.4 m/s so that the wind velocity passing through the smooth passages of the heat sinks u_{c} will be 6.5, 8.0, 10.0, and 12.2 m/s, respectively. At the outlet of the computational domain, a pressure boundary condition is employed. The interface between

Table 3. Boundary conditions

Inlet	$U = \text{const}$, $v = w = 0$, $T = \text{const}$
Outlet	$\frac{\partial u_i}{\partial x} = \frac{\partial T}{\partial x} = 0$
Eight surfaces of the extended region	Slip and adiabatic wall
Interface between air and solid	No-slip, no thermal resistance
Other surfaces	Adiabatic

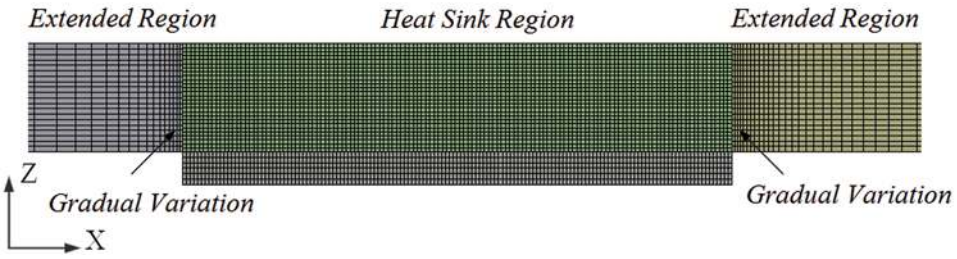

Figure 3. Mesh for the computational domain (color figure available online).

the solid and the fluid is a no-slip wall with no thermal resistance. An iso-heat-flux thermal boundary condition is employed on the bottom surface of each type of heat sink, and the total heat load is 10 W. Slip and adiabatic wall conditions are provided on all the other confined walls. The boundary conditions assigned for the computational domain are tabulated in Table 3.

The grid systems for all heat sink models are built by Ansys Meshing. It is known that for flow-aligned geometries, hex mesh can provide higher-quality solutions with fewer cells than a comparable tet-mesh. Therefore, a structured hex-mesh is carefully created, aligning the mesh with the flow to reduce false diffusion. In the extended parts, a coarser grid is adopted to conserve computational resources. A grid system with a gradual variation in and after the fin region is used to avoid the undesirable effect of an abrupt grid width change in the computing region. The grid system for one of the heat sinks is shown in Figure 3.

Grid independence tests were made carefully by recursive refinement and comparison between the numerical simulation results. The above process was repeated until the variation of pressure drop and thermal resistance was less than 0.5%, so that the numerical predictions can be regarded as grid-independent. With the turbulence predictions employed, the meshes near the fluid solid interface are fine enough to resolve the flow behavior close to the no-slip wall. For all simulation cases, y^+ values in the near-wall region are less than 1.

3. RESULTS AND DISCUSSION

The numerical analysis in this section consists of five parts. First, the parameters used to evaluate the performance of the heat sinks are defined. Next, the computational model and the method adopted in current numerical simulations are verified and validated by comparing the CFD results with the experimental data. Then the streamlines and temperature contours of different types of PPFHSs in a plane normal to z-axis are compared. After having a qualitative view into the flow behavior and heat transfer phenomenon, the thermal and hydraulic performances of different types of PPFHSs are compared with plate fin and pin fin heat sinks quantitatively by means of Nusselt number and pressure drop, respectively. Finally, a comprehensive comparison is made to evaluate the synthetical performance of all types of PPFHSs.

3.1. Parameter Definitions

Definitions are presented for the characteristic quantities which will be used in the presentations of numerical results.

The thermal resistance of the heat sinks R_{th} is defined by

$$R_{th} = \frac{\Delta T}{Q} \tag{13}$$

It should be noted that Jonsson and Moshfegh [23] and Yu [28] defined the temperature difference ΔT differently. Jonsson and Moshfegh [23] defined ΔT as the difference between the average temperature on the base and the inlet air temperature, while Yu [28] defined it as the difference between the highest temperature on the base and the inlet air temperature. Given the different definitions of ΔT, when the simulation results are validated by comparison with the experimental data, the corresponding definitions of ΔT are adopted for different heat sinks, while when quantitative comparisons are made for all types of heat sinks, ΔT is uniformly defined using Yu's [28] definition.

The average Nusselt number N_u is defined by

$$\mathrm{Nu} = \frac{QD_h}{A_P \Delta T \lambda_f} \tag{14}$$

where D_h is the hydraulic diameter of the wind tunnel with no bypass suggested by Jonsson and Moshfegh [23], which is

$$D_h = 2 \cdot CH \cdot CB/(CH + CB) \tag{15}$$

The friction factor f is defined as

$$f = \frac{\Delta p}{0.5 \rho u_{in}^2} \cdot \frac{D_h}{4L} \tag{16}$$

The Reynolds number is defined as

$$\mathrm{Re} = \frac{\rho u_{in} D_h}{\mu} \tag{17}$$

To evaluate the comprehensive performance of all the heat sinks, the heat transfer effectiveness factor η_{eff} is defined as

$$\eta_{\mathrm{eff}} = \frac{\mathrm{Nu}/\mathrm{Nu}_\infty}{(f/f_\infty)^{1/3}} \tag{18}$$

where the comparative references of heat transfer Nu_∞ and friction factor f_∞ are selected as the levels in smooth circular tube with fully developed flow, which is defined as follows.

Dittus-Boelter correlation for turbulent flow

$$\mathrm{Nu}_\infty = 0.023\ \mathrm{Re}^{0.8}\ \mathrm{Pr}^{0.4} \tag{19}$$

Blasius equation for turbulent flow

$$f_\infty = 0.079\ \mathrm{Re}^{-0.25} \tag{20}$$

3.2. Validation and Verification

To verify the computational model and the method adopted in current numerical simulation, preliminary computations were first conducted for the plate fin, pin fin and circular plate-pin fin heat sinks, the dimensions of which are the same as the heat sinks tested by Jonsson and Moshfegh [23] and by Yu [28].

The comparisons of thermal resistance and pressure drop between the current simulation results and the experimental data are shown in Figure 4. We found that the maximum deviations in thermal resistance and pressure drop are less than 5% for all three kinds of heat sinks. Our predicted results and the experimental data agree very well, demonstrating the accuracy of the physical model and the adopted numerical method.

3.3. Qualitative Comparison Between Different PPFHSs

For the present CFD simulation, the velocity streamlines and temperature fields are three-dimensional, so the presentation of these parameters are done for a plane normal to the z-axis. Figure 5 provides insight into the local distributions of the streamlines for the section in the x-y plane through $z = 8\,\mathrm{mm}$ for $u_c = 10\,\mathrm{m/s}$. It can be clearly seen from Figure 5 that there are some recirculation zones in the rear pin portion. It is known that a dead zone is characterized by the stationary recirculation region that forms when the flow separates at the rear portion of a pin and reattaches at the front of the following pin. The dead flow zone will decrease the convective heat transfer to the pin but enhance the heat transfer to the plate fin.

The flow seperates at different angles for different types of pins. The angle between the stagnation point and the separation point for circular and square pins is smaller than the streamline-shaped pins. The seperation from a square pin is the most prominent of all five types. By comparing the streamline patterns of all five types of pins, it can be seen that there are larger scale vortices in the rear region of circular and square pins, especially for a square pin, due to the sharp corners.

The temperature contours in the flow channels around the pin fins are shown in Figure 6 for $u_c = 10\,\mathrm{m/s}$. Compared with the streamline figures, an extra image showing the temeperature distribution in the x-z plane through $y = 3.25$ is added to the figures of temperature countours. Since the temperature variation along the pins is qualitatively similar for all the types of PPFHS, only the x-z images for circular PPFHS are presented.

It can be seen that all fluid-solid interfaces, including the surface around the pins, the surface covering the base, and interfaces between fluid and the plate fins are covered by a thermal boundary layer, the development of which is similar to the velocity boundary layer. Due to the existence of pins in the heat sink channels,

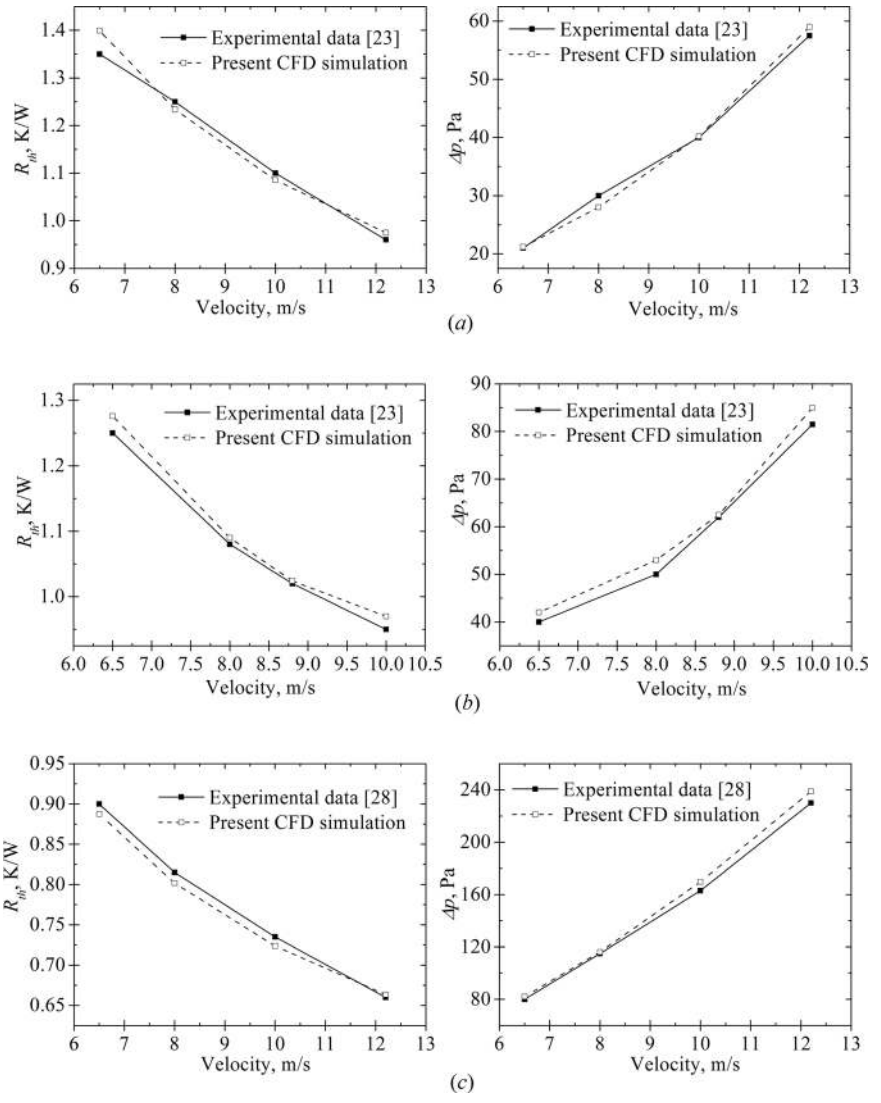

Figure 4. Comparison between the present CFD results and experimental data. (*a*) Plate fin heat sink; (*b*) pin fin heat sink; and (*c*) plate-pin fin heat sink.

the development of the thermal boundary layers which cover the plate fins is hindered periodically. Since the top wall is set to be free slip and adiabatic, no boundary layer develops there.

3.4. Quantitative Comparison Between Different PPFHSs

To get a more quantitative impression, the comparisons of flow and heat transfer characteristics of the PPFHSs with the plate fin and pin fin heat sinks in terms of

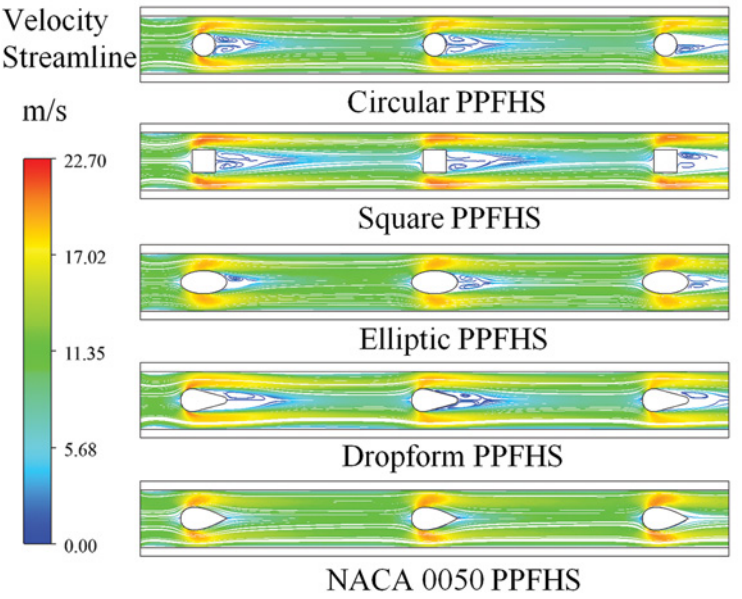

Figure 5. Streamline patterns in the plane $z = 8\,\text{mm}$, $u_c = 10\,\text{m/s}$ (color figure available online).

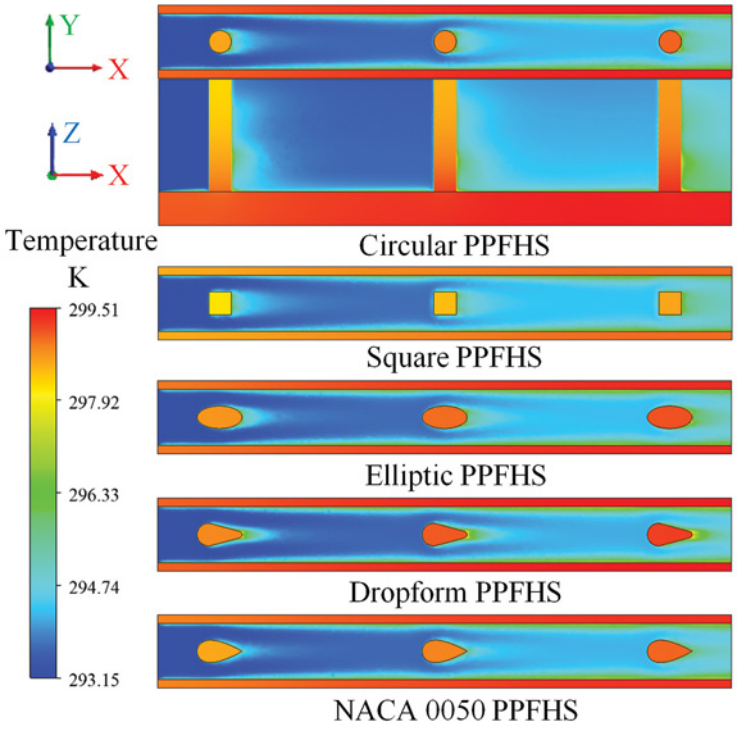

Figure 6. Temperature contours in the plane $z = 8\,\text{mm}$, $u_c = 10\,\text{m/s}$ (color figure available online).

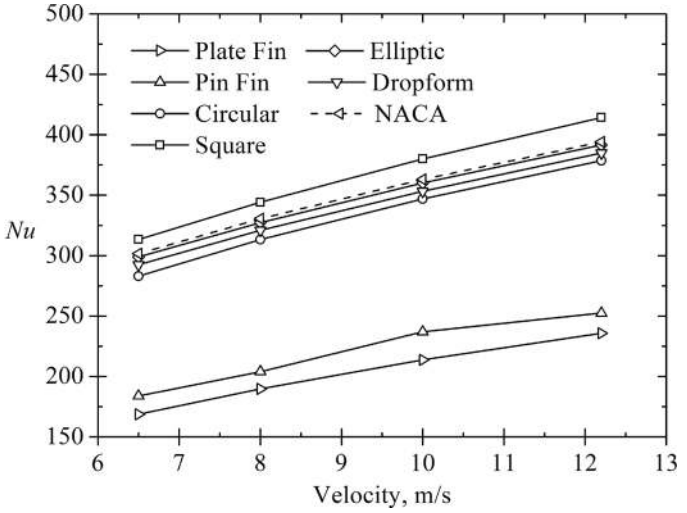

Figure 7. Nusselt numbers of heat sinks as a function of wind velocity, $b/S_f = 0.4$.

Nusselt number and pressure drop are plotted in Figures 7–10. In Figures 7 and 8, the dimensionless width of all pins is set to be 0.4, and the wind velocity increases from 6.5 m/s to 12.2 m/s. In Figures 9 and 10, the wind velocity is set to be 6.5 m/s and the dimensionless width of all the pins increases from 0.3 to 0.6.

From Figure 7, it is clear that the pin fin heat sink has a higher Nusselt number (around 9%) than the plate fin heat sink, which agrees with the experimental data of Jonsson and Moshfegh [23]. By placing pin fins in the channels of plate fin heat sinks, the heat transfer capability increases greatly with the Nusselt number being over 60%

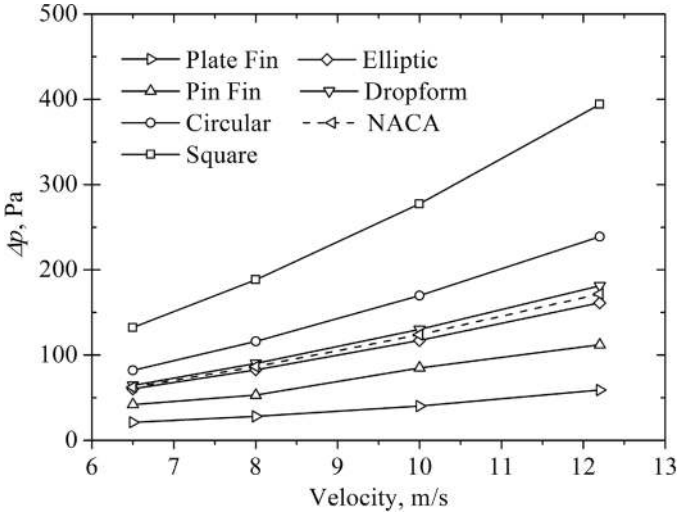

Figure 8. Pressure drops of heat sinks as a function of wind velocity, $b/S_f = 0.4$.

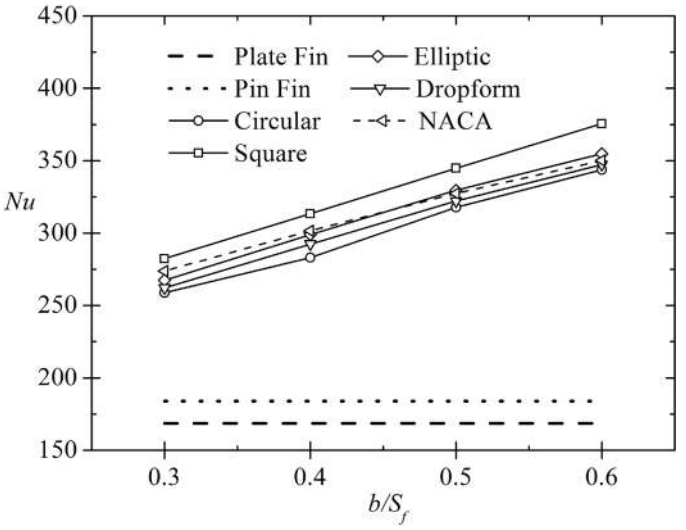

Figure 9. Nusselt numbers of heat sinks as a function of b/S_f, $u_c = 6.5\,\mathrm{m/s}$.

higher than the plate fin heat sinks. The square type PPFHS has the highest Nu compared with the other heat sinks. The augmentation of Nu is over 75% higher than PFHS and the maximum augmentation reaches 86%. The NACA type and the elliptic type of PPFHSs present similar heat transfer characteristics, yielding an average increment of 71%. The dropform type PPFHS has the lowest Nu except for the circular type, with average augmentation of 68% and 63% for the former and latter, respectively.

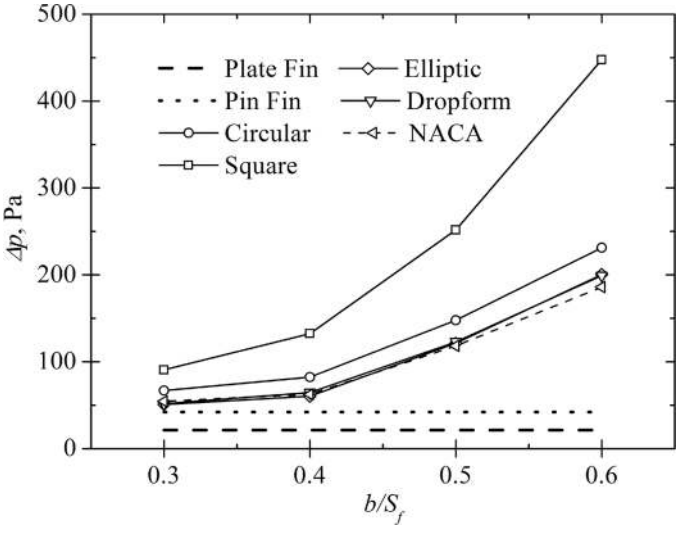

Figure 10. Pressure drops of heat sinks as a function of b/S_f, $u_c = 6.5\,\mathrm{m/s}$.

Comparisons of pressure drop are presented in Figure 8. The pin fin heat sink has about 97% higher pressure drop than the plate fin heat sink. For the PPFHSs, it is not surprising that the square type PPFHS has the highest pressure drop compared to the other types of PPFHSs. The pressure drop of a square PPFHS is over 525% higher than that of a PFHS at the same wind velocity. The pressure drop of the circular type PPFHS is much lower compared with the square type, but is still about 307% higher than the PFHS. The streamline-shaped pins (dropform, NACA 0050, elliptic) increase the pressure drop by a much smaller percentage, having an average increase of 214%, 201% and 186%, respectively. It should be noted that the NACA type of PPFHS doesn't show any advantage regarding the pressure drop compared with the other streamline-shaped types of PPFHSs. The elliptic type shows a shightly better hydraulic performance than the NACA type. The reason this happened is that the maximum thickness as a fraction of the chord for the NACA profile chosen in the present work is far higher than the optimum ratio which is of the order of 0.2. With the blockage area being the same and the pressure drop being primarily form drag, the lack of large differences for streamline-shaped types of PPFHSs is not unexpected.

Figures 9 and 10 show the effect of the dimensionless width of the pins b/S_f on the Nusselt number and pressure drop for different plate-pin fin heat sinks. Just as expected (shown in Figure 9), the Nu numbers of all five types of plate-pin fin heat sinks increase as b/S_f increases. With the increase of b/S_f, the square type PPFHS keeps showing the highest Nusselt number, followed by the NACA type and elliptic type, which have a similar Nu. The dropform type and ciruclar type have a lower Nu number, with the dropform type outweighing the circular type slightly. On the other hand, as shown in Figure 10, the pressure drops also increase as b/S_f increases and still, the square type PPFHS has the highest pressure drop followed by the circular type. The streamline-shaped types of PPFHSs have a similar pressure drop, much lower than the square and circular types. It's worth noting that the Nu numbers for all PPFHSs have a similar increasing trend as b/S_f increases, while the pressure drops for the PPFHSs are diverging with the increase of b/S_f, which indicates the existence of an optimum width of pins if both the heat transfer augmentation and the friction-loss increase are taken into consideration.

3.5. Comprehensive Performance Comparison

Figures 7–10 compare the heat sinks with various shapes of pin cross-section and different dimensionless pin widths regarding heat transfer enhancement and pressure drop increment separately. However, increasing Nusselt number is accompanied by increasing pressure drop which is undesirable. Thus, based only on Figures 7–10, it is almost impossible to come to a final conclusion as to which type of heat sink performs better than the others if both the heat transfer enhancement and power consumption are considered simultaneously. Therefore, a comprehensive performance comparison should be made to evaluate the effectiveness of different types of heat sinks.

A comprehensive comparison of heat transfer effectiveness factor is made and shown in Figures 11–13 using the definition given by Eq. (18). The geometric configuration that has the maximum η_{eff} can dissipate more heat while consuming less power and keeping the temperature of the base at a lower value.

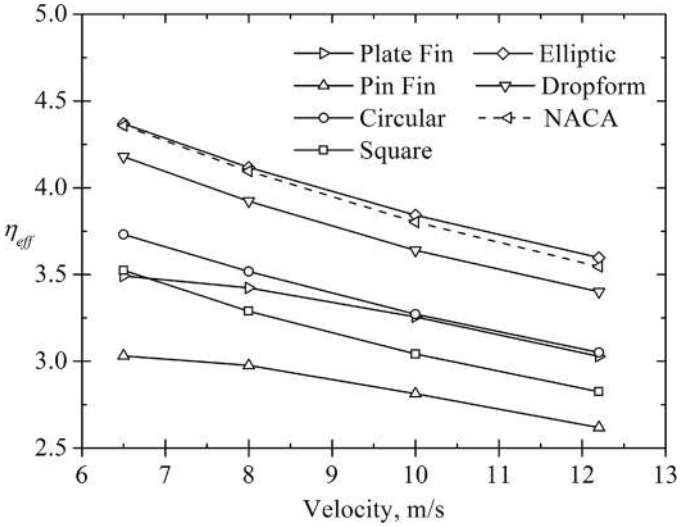

Figure 11. Heat sink performance η_{eff} as a function of wind velocity, $b/S_f = 0.4$.

From Figure 11, it is easy to see that the plate fin heat sink has a higher heat transfer effectiveness factor than the pin fin heat sink in the tested wind velocity region and that not all five types of PPFHSs have higher comprehensive performance than the plate fin heat sink. The one which performs worse than the plate fin heat sink is the square type PPFHS, since planting the square pin fins in the channel of a plate fin heat sink leads to a considerably higher pressure drop which offsets its heat transfer enhancement potential. The efficiency of the circular type is much

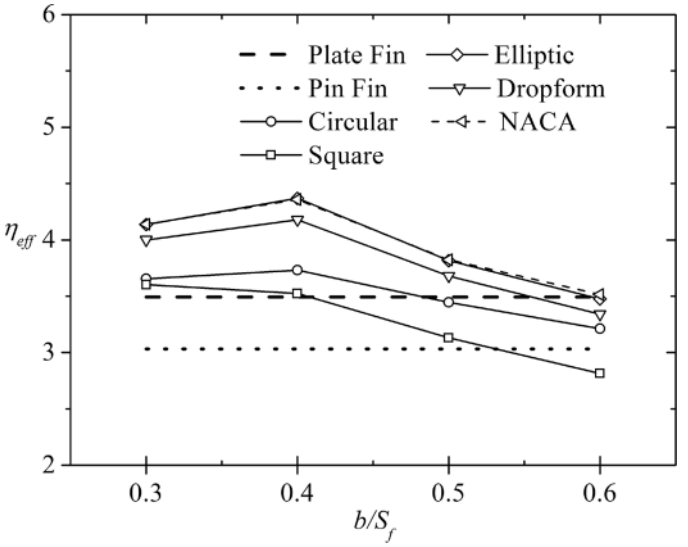

Figure 12. Heat sink performance η_{eff} as a function of b/S_f, $u_c = 6.5\,\text{m/s}$.

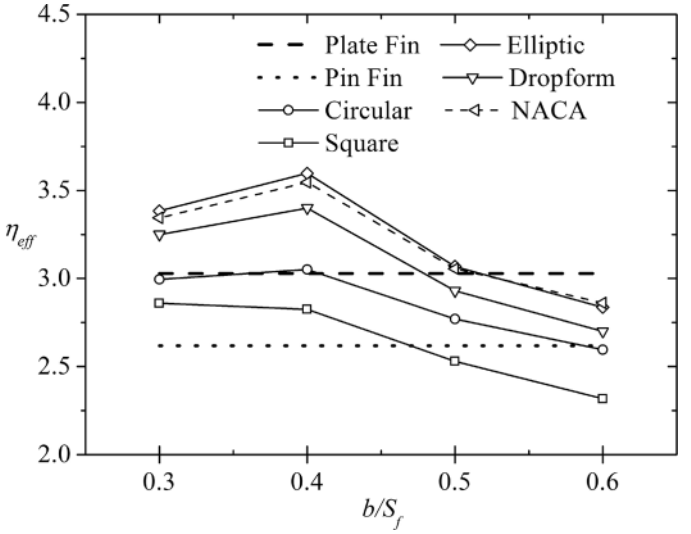

Figure 13. Heat sink performance η_{eff} as a function of b/S_f, $u_c = 12.2\,\text{m/s}$.

better than the square type. When the wind velocity is 6.5 m/s, the effectiveness factor of the circular type is about 7% higher than the plate fin heat sink, while as the wind velocity increases, the advantage of the circular type PPFHS diminishes but is still higher than the plate fin heat sink. Yu et al. [28] reached a similar conclusion based on their experimental data.

By employing streamline-shaped pins, the effectiveness of this new compound heat sink takes a step forward and is much higher than the original circular type. The elliptic type PPFHS has the best overall performance (around 20.5% over the plate fin heat sink), outweighing the NACA type a little, which has about 19.5% higher η_{eff} than PFHS. The elliptic pins minimize the pressure drop across the heat sink by reducing the vortex effects and enhance the thermal performance by maintaining large exposed surface area available for heat transfer. The dropform type PPFHS performs the worst among the three types of streamline-shaped PPFHSs, but still shows almost 15% higher η_{eff} than the plate fin heat sink.

Figures 12 and 13 present a comparison of η_{eff} for different heat sinks as a function of the dimensionless width of pins. The wind velocity is set to 6.5 m/s and 12.2 m/s in Figures 12 and 13, respectively. These two pictures reveal three main pieces of information.

1. It is obvious that the effectiveness factor of all the PPFHSs peaks at $b/S_f = 0.4$ except the square type. For the square type PPFHS, it seems that the smaller the b/S_f is the higher η_{eff} it has. As the b/S_f increases from 0.4 to 0.6, the effectiveness of all the PPFHSs decreases.
2. Figure 12 shows that when wind velocity is 6.5 m/s b/S_f shouldn't be larger than 0.6, since when $b/S_f = 0.6$, all five types of PPFHSs have no advantage over the plate fin heat sink. As the wind velocity increases, the maximum allowable

dimensionless width of the pins decreases. From Figure 13, it can be seen that when the wind velocity is 12.2 m/s, a b/S_f no higher than 0.5 is recommended.

3. With the increase of b/S_f, the elliptic type and NACA type of PPFHSs continue to perform the best, with the elliptic type having a little higher η_{eff} than the NACA type, followed by the dropform type. The square type PPFHS, has the lowest η_{eff} among the five types of PPFHSs, and the η_{eff} curve as a function of b/S_f for the circular type lies between those of the dropform type and square type.

The above analysis indicates that choosing a proper pin fin cross-section profile and dimensionless width of pins plays an important role in increasing the overall performance of this new compound plate-pin fin heat sink. The employment of the streamline-shaped pins with appropriate ratio of pin width to the plate fin spacing considerably increases the synthetical performance of PPFHS, and makes them highly competitive heat dissipation solutions.

4. CONCLUSION

By placing pin fins in the flow channel of a smooth plate fin heat sink, the thermal and fluid dynamic boundary layers are interrupted periodically and the fluid parts with different temperatures mix better. The present article describes an effort to numerically analyze the forced convective heat transfer through the channels of different types of plate-pin fin heat sinks. Twenty-two types of heat sink models in total, including the commonly used plate fin and pin fin heat sinks, were simulated. Based on the results of the present study, the following conclusions can be drawn.

1. Placing pin fins in the flow channels is a good way to overcome the intrinsic shortcomings of smooth plate fin heat sinks. All of the tested PPFHSs have higher Nusselt numbers as well as higher pressure drops than plate fin and pin fin heat sinks. However, considering the heat transfer enhancement and power consumption simultaneously, not all PPFHSs have better overall performance than the plate fin heat sink.
2. The heat transfer enhancement of a square type PPFHS, which is the highest of all the heat sinks considered, is offset by its high pressure drop, leading to lower heat transfer effectiveness than the plate fin heat sink. The effectiveness of the circular type is higher than the square type; however, as the wind velocity increases, the advantage of the circular type PPFHS diminishes.
3. The streamline-shaped types of PPFHSs perform much better than the circular and square types, and among them the elliptic and NACA 0050 types have a similar overall performance, with the elliptic type outweighing the NACA type slightly, followed by the dropform type.
4. The effectiveness factor of all the PPFHSs peaks at $b/S_f = 0.4$, except the square type, indicating the existence of an optimum width for pins. Further increasing b/S_f will decrease the effectiveness of PPFHSs.
5. In the tested velocity range, the performance of the five types of PPFHSs can be ordered as follows: elliptic $\approx$ NACA>dropform>circular>plate fin heat sink> square>pin fin heat sink.

A full optimization was not done in this work, primarily because of the computational expense. There are a number of other factors that need further evaluation before one can say that these results are promising but not definitive. The large number of parameters and consequent numbers of trials needed for optimization will require more than a full numerical approach. We leave this to another study.

REFERENCES

1. R. W. Knight, J. S. Goodling, and D. J. Hall, Optimal Thermal Design of Forced Convection Heat Sinks-Analytical, *J. Electronic Packaging*, vol. 113, no. 3, pp. 313–321, 1991.
2. R. W. Knight, D. J. Hall, J. S. Goodling, and R. C. Jaeger, Heat Sink Optimization with Application to Microchannels, *Components, Hybrids, and Manufacturing Tech., IEEE Trans.*, vol. 15, no. 5, pp. 832–842, 1992.
3. R. W. Knight, J. S. Goodling, and B. E. Gross, Optimal Thermal Design of Air Cooled Forced Convection Finned Heat Sinks-Experimental Verification, *Components, Hybrids, and Manufacturing Techn., IEEE Transa.*, vol. 15, no. 5, pp. 754–760, 1992.
4. P. Teertstra, M. M. Yovanovich, and J. R. Culham, Analytical Forced Convection Modeling of Plate Fin Heat Sinks, *J. Electronics Manufacturing*, vol. 10, Compendex, pp. 253–261, 2000.
5. D. Copeland, Optimization of Parallel Plate Heatsinks for Forced Convection, *Proc. Annual IEEE Semiconductor Thermal Measurement and Management Symposium, Compendex*, pp. 266–272, IEEE, San Jose, CA, USA, 2000.
6. J. R. Culham and Y. S. Muzychka, Optimization of Plate Fin Heat Sinks using Entropy Generation Minimization, *Components and Packaging Technologies, IEEE Trans.*, vol. 24, no. 2, pp. 159–165, 2001.
7. M. Iyengar and A. Bar-Cohen, Least-Energy Optimization of Forced Convection Plate-Fin Heat Sinks, *Components and Packaging Technologies, IEEE Trans.*, vol. 26, no. 1, pp. 62–70, 2003.
8. K.-T. Chiang, Optimization of the Design Parameters of Parallel-Plain Fin. Heat Sink Module Cooling Phenomenon Based on the Taguchi Method, *Int. Commu. Heat and Mass Transfer*, vol. 32, no. 9, pp. 1193–1201, 2005.
9. E. M. Sparrow, J. W. Ramsey, and C. A. C. Altemani, Experiments on In-Line Pin Fin Arrays and Performance Comparisons with Staggered Arrays, *J. Heat Transfer*, vol. 102, no. 1, pp. 44–50, 1980.
10. E. M. Sparrow and S. S. Kang, Longitudinally-Finned Cross-Flow Tube Banks and their Heat Transfer and Pressure Drop Characteristics, *Int. J. Heat and Mass Transfer*, vol. 28, no. 2, pp. 339–350, 1985.
11. E. M. Sparrow and V. B. Grannis, Pressure Drop Characteristics of Heat Exchangers Consisting of Arrays of Diamond-Shaped Pin Fins, *Int. J. Heat and Mass Transfer*, vol. 34, no. 3, pp. 589–600, 1991.
12. C. L. Chapman, S. Lee, and B. L. Schmidt, Thermal Performance of an Elliptical Pin Fin Heat Sink, *Proc. IEEE Semiconductor Thermal Measurement & Management Symposium,* pp. 24–31, IEEE, San Jose, CA, USA, 1994.
13. Q. Li, Z. Chen, U. Flechtner, et al., Heat Transfer and Pressure Drop Characteristics in Rectangular Channels with Elliptic Pin Fins, *Int. J. Heat and Fluid Flow*, vol. 19, no. 3, pp. 245–250, 1998.
14. K.-S. Yang, W.-H. Chu, I.-Y. Chen, et al., A Comparative Study of the Airside Performance of Heat Sinks Having Pin Fin Configurations, *Int. J. Heat and Mass Transfer*, vol. 50, no. 23–24, pp. 4661–4667, 2007.

15. A. Horvat and I. Catton, Numerical Technique for Modeling Conjugate Heat Transfer in an Electronic Device Heat Sink, *Int. J. Heat and Mass Transfer*, vol. 46, no. 12, pp. 2155–2168, 2003.
16. A. Horvat and B. Mavko, Hierarchic Modeling of Heat Transfer Processes in Heat Exchangers, *Int. J. Heat and Mass Transfer*, vol. 48, no. 2, pp. 361–371, 2005.
17. K. Park, D.-H. Choi, and K.-S. Lee, Numerical Shape Optimization for High Performance of a Heat Sink with Pin-Fins, *Numer. Heat Transfer A*, vol. 46, no. 9, pp. 909–927, 2004.
18. H.-T. Chen, P.-L. Chen, J.-T. Horng, and Y.-H. Hung, Design Optimization for Pin-Fin Heat Sinks, *J. Electronic Packaging*, vol. 127, no. 4, pp. 397–406, 2005.
19. W. A. Khan, J. R. Culham, and M. M. Yovanovich, Optimization of Pin-Fin Heat Sinks using Entropy Generation Minimization, *Components and Packaging Technologies, IEEE Tran.*, vol. 28, no. 2, pp. 247–254, 2005.
20. W. A. Khan, J. R. Culham, and M. M. Yovanovich, Optimization of Pin-Fin Heat Sinks in Bypass Flow using Entropy Generation Minimization Method, *J. Electronic Packaging*, vol. 130, no. 3, pp. 031010–7, 2008.
21. K.-T. Chiang and F.-P. Chang, Application of Response Surface Methodology in the Parametric Optimization of a Pin-Fin Type Heat Sink, *Int. Comm. Heat and Mass Transfer*, vol. 33, no. 7, pp. 836–845, 2006.
22. K.-T. Chiang, F.-P. Chang, and T.-C. Tsai, Optimum Design Parameters of Pin-Fin Heat Sink using the Grey-Fuzzy Logic Based on the Orthogonal Arrays, *Intl. Comm. Heat and Mass Transfer*, vol. 33, no. 6, pp. 744–752, 2006.
23. H. Jonsson and B. Moshfegh, Modeling of the Thermal, and Hydraulic Performance of Plate Fin, Strip Fin, and Pin Fin Heat Sinks-Influence of Flow Bypass, *Components and Packaging Technologies, IEEE Trans.*, vol. 24, no. 2, pp. 142–149, 2001.
24. D. Soodphakdee, M. Behnia, and D. W. Copeland, A Comparison of Fin Geometries for Heatsinks in Laminar Forced Convection: Part I—Round, Elliptical, and Plate Fins in Staggered, and In-Line Configurations, *Int. J. Microcircuits and Electronic Packaging*, vol. 24, no. 1, pp. 68–76, 2001.
25. S. J. Kim, D.-K. Kim, and H. H. Oh, Comparison of Fluid Flow and Thermal Characteristics of Plate-Fin and Pin-Fin Heat Sinks Subject to a Parallel Flow, *Heat Transfer Eng.*, vol. 29, no. 2, pp. 169–177, 2008.
26. X. L. Yu, Q. K. Feng, and Q. P. Liu, Research on the Heat Transfer and Flow Performance of a Composite Heat Sink, *J Xi'an Jiaotong Univ.*, vol. 37, no. 4, pp. 670–673, 2003.
27. X. L. Yu, Q. K. Feng, and J. M. Feng, Research on Thermal Performance of Plate-Pin Fin Heat Sink, *J Xi'an Jiaotong Univ.*, vol. 38, no. 11, pp. 1114–1118, 2004.
28. X. Yu, J. Feng, Q. Feng, and Q. Wang, Development of a Plate-Pin Fin Heat Sink and its Performance Comparisons with a Plate Fin Heat Sink, *App. Ther. Eng.*, vol. 25, no. 2–3, pp. 173–182, 2005.
29. Y.-T. Yang and H.-S. Peng, Numerical Study of Thermal and Hydraulic Performance of Compound Heat Sink, *Numer. Heat Transfer A*, vol. 55, no. 5, pp. 432–447, 2009.
30. Y.-T. Yang and H.-S. Peng, Investigation of Planted Pin Fins for Heat Transfer Enhancement in Plate Fin Heat Sink, *Microelectronics Reliability*, vol. 49, no. 2, pp. 163–169, 2009.
31. N. E. Jacobs, *Tests of Six Symmetrical Airfoils in the Variable Density Wind Tunnel*, NASA Report no. 385, NASA, Washington, D.C., 1931.
32. N. E. Jacobs, K. E. Ward, and R. M. Pinkerton, *The Characteristics of 78 Related Airfoil Sections from Tests in the Variable-Density Wind Tunnel*, NASA Report no. 460, NASA, Washington, D.C., 1933.
33. J. Moran, *An Introduction to Theoretical and Computational Aerodynamics*, chap. 4, Dover Publications, New York, 2003.

34. J. D. Anderson, Governing Equations of Fluid Dynamics, In J. D. Anderson, G. E. Degrez, J. Degroote, et al. (eds.), *Computational Fluid Dynamics*, 3rd ed., chap. 2, Springer, Heidelberg, Germany, 2009.
35. B. R. Baliga and N. Atabaki, Control-Volume-Based Finite-Difference, and Finite-Element Methods, In W. J. Minkowycz, E. M. Sparrow, J. Y. Murthy (eds.), *Handbook of Numerical Heat Transfer*, 2nd ed., chap. 6, Wiley, Hoboken, New Jersey, 2009.
36. S. V. Patankar, *Numerical Heat Transfer and Fluid Flow*, chap. 2, Hemisphere Publishing Corp., Washington, D.C., 1980.
37. F. R. Menter and T. Esch, Elements of Industrial Heat Transfer Predictions, *Proc. 16th Bazilian Congress of Mechanical Engineering (COBEM)*, Uberlandia, Brazil, 2001.
38. J. E. Bardina, P. G. Huang, and T. J. Coakley, *Turbulence Modeling Validation, Testing, and Development*, NASA Technical Memorandum, Moffett Field, CA, 1997.
39. F. R. Menter, Two-Equation Eddy-Viscosity Turbulence Models for Engineering Applications, *AIAA J.*, vol. 32, no. 8, pp. 1598–1605, 1994.
40. F. R. Menter, M. Kuntz, and R. Langtry, Ten Years of Industrial Experience with the SST Turbulence Model, *Turbulence, Heat and Mass Transfer*, vol. 4, pp. 625–632, 2003.
41. Ansys CFX-12.1, Ansys Inc., Canonsburg, PA, 2009.